Stellar Kinematics of Boxy Bulges: Large-Scale Bars and Inner Disks

Aeree Chung¹

Department of Astronomy, Columbia University, 550 West 120th Street, 1411 Pupin Hall, MC 5246, New York, NY 10027

archung@astro.columbia.edu

and

M. Bureau²

Columbia Astrophysics Laboratory, 550 West 120th Street, 1027 Pupin Hall, MC 5247, New York, NY 10027

bureau@astro.columbia.edu

ABSTRACT

Long-slit stellar kinematic observations were obtained along the major-axis of 30 edge-on spiral galaxies, 24 with a boxy or peanut-shaped (B/PS) bulge and 6 with other bulge types for comparison. B/PS bulges are identified in at least 45% of highly inclined systems and a growing body of theoretical and observational work suggests that they are the edge-on projection of thickened bars. Profiles of the mean stellar velocity V, the velocity dispersion σ , as well as the asymmetric (h_3) and symmetric (h_4) deviations from a pure Gaussian are presented for all objects. Comparing those profiles with stellar kinematic bar diagnostics developed from N-body simulations, we find bar signatures in 24 of our sample galaxies (80%). Galaxies with a B/PS bulge typically show a double-hump rotation curve with an intermediate dip or plateau. They also frequently show a rather flat central velocity dispersion profile accompanied by a secondary peak or

¹Send offprint requests to Aeree Chung: archung@astro.columbia.edu

²Hubble Fellow

plateau, and numerous galaxies have a local central σ minimum ($\gtrsim 40\%$). The h_3 profiles display up to three slope reversals. Most importantly, h_3 is normally correlated with V over the presumed bar length, contrary to expectations from axisymmetric disks. These characteristic bar signatures strengthen the case for a close relationship between B/PS bulges and bars and leave little room for other explanations of the bulges' shape. We also find that h_3 is anti-correlated with V in the very center of most galaxies ($\gtrsim 60\%$), indicating that these objects additionally harbor cold and dense decoupled (quasi-)axisymmetric central stellar disks, which may be related to the central light peaks. These central disks coincide with previously identified star-forming ionized-gas disks (nuclear spirals) in gas-rich systems, and we argue that they formed out of gas accumulated by the bar at its center through inflow. As suggested by N-body models, the asymmetry of the velocity profile (h_3) appears to be a reliable tracer of asymmetries in disks, allowing us to discriminate between axisymmetric and barred disks seen in projection. B/PS bulges (and thus a large fraction of all bulges) appear to be made-up mostly of disk material which has acquired a large vertical extent through bar-driven vertical instabilities. Their formation is thus probably dominated by secular evolution processes rather than merging.

Subject headings: galaxies: kinematics and dynamics — galaxies: bulges — galaxies: spiral — galaxies: structure — galaxies: formation — galaxies: evolution

1. Introduction

The number of edge-on disk galaxies with a boxy or peanut-shaped (B/PS) bulge is known to be significant. In fact, the fraction of these objects has continuously increased as sample selection, data, and classification criteria improved (see Jarvis 1986; de Souza & dos Anjos 1987; Shaw 1987; Dettmar & Barteldrees 1988; Lütticke, Dettmar, & Pohlen 2000a,b). Recently, Lütticke et al. (2000a) classified ≈ 1350 edge-on disk galaxies and found 45% of B/PS bulges, with a fraction higher than 40% for all morphological types from S0 to Sd. This was the first study to report such a large incidence of B/PS bulges in very late type systems, but it is also the largest and most homogeneous. B/PS bulges are therefore common, but they are only seen in highly inclined systems ($i \gtrsim 75^{\circ}$; e.g. Shaw, Dettmar, & Barteldrees 1990), indicating that their shape is mainly related to the vertical distribution of light.

Several scenarios have been suggested to explain the structure and formation of B/PS bulges. They can be divided into two main categories: axisymmetric accretion and non-

axisymmetric bar buckling models. Binney & Petrou (1985) and Rowley (1988; but see also May et al. 1985) showed that it is possible to form axisymmetric cylindrically rotating B/PS bulges from the accretion of one or (more likely) many satellite galaxies onto a larger galaxy host. As pointed out by Binney & Petrou (1985), however, the particular alignment required puts too many constraints on the orbits, angular momenta, and relative masses of the galaxies, and this process appears unlikely in view of the high incidence of B/PS bulges. Moreover, satellite galaxies are not preferentially observed around galaxies with a B/PS bulge (Shaw 1987). Using N-body simulations, Combes & Sanders (1981) first suggested that B/PS bulges could be due to the thickening of bars in the disks of spiral galaxies. They showed that soon after a bar develops through the usual bar instability, it buckles, thickens, and settles with a larger velocity dispersion and thickness. When highly inclined, the bar then appears peanut-shaped when seen side-on (i.e. perpendicular to the bar), boxy-shaped when seen at intermediate angles, and almost round when seen end-on (i.e. parallel to the bar). It is also largely cylindrically rotating. Combes & Sanders's (1981) results were later confirmed and improved upon by many studies (e.g. Combes et al. 1990; Raha et al. 1991; Athanassoula & Misiriotis 2002) and they are now universally accepted. The three-dimensional (3D) orbital structure of these bars has just been investigated in a series of papers (Skokos, Patsis, & Athanassoula 2002a,b; Patsis, Skokos, & Athanassoula 2002, 2003; but see also Pfenniger 1984; Pfenniger & Friedli 1991), allowing a more detailed comparison of models with high spatial resolution images.

There are several observational studies supporting the connection between B/PS bulges and bars. Most important for this work, Kuijken & Merrifield (1995) suggested that bars could be detected in edge-on galaxies from their (projected) kinematic signature. In their pioneering study of two spirals with a peanut-shaped bulge (NGC 5746 and NGC 5965), Kuijken & Merrifield (1995) found a characteristic "figure-of-eight" bar signature in their position-velocity diagrams (PVDs; the projected density of material as a function of lineof-sight velocity and projected position). Although the interpretation of this signature was ultimately flawed, hydrodynamical simulations by Athanassoula & Bureau (1999) confirmed its relationship to bars and showed how it can be used to identify and characterize edge-on bars from gas kinematics. In a study of emission-line spectra for 10 edge-on spirals with various types of bulges, Merrifield & Kuijken (1999) later confirmed the link between B/PS bulges and bars. Bureau & Freeman (1999; see also Bureau 1998) also presented ionized-gas PVDs for 23 edge-on galaxies, 17 with a B/PS bulge and 6 with other types of bulges (mostly spheroidal). Using Athanassoula & Bureau's (1999) diagnostics, they found bar signatures in 14 of 17 galaxies with a B/PS bulge ($\approx 80\%$) and in none of the galaxies with a more spheroidal bulge.

In spite of the aforementioned studies, our knowledge of the stellar kinematics of B/PS

bulges and their hosts remains limited. This probably arises because the gas is a more practical tracer of the barred potential, being both easier to observe and reacting more strongly than the stars to asymmetries (shocks). Studying the stars directly is nevertheless essential as B/PS bulges are stellar structures and, when comparing to N-body simulations, stellar kinematics largely bypasses issues such as the selection of an optimal gaseous tracer (H α , CO, H I, etc), star formation, and (for gas-poor objects) the response of the orbital structure to a massive gas disk (e.g. Berentzen et al. 1998).

Existing stellar kinematic studies of B/PS bulges are limited to a few objects and have largely focused on the issue of cylindrical rotation, using slits offset from the major-axis or perpendicular to it (e.g. Bertola & Capaccioli 1977; Kormendy & Illingworth 1982; Rowley 1986; Jarvis 1987; Shaw 1993a; Shaw, Wilkinson, & Carter 1993). As noted above, however, this is consistent with both axisymmetric and barred configurations, and so does not discriminate between the two dominant formation scenarios. We advocate here instead the new kinematic bar diagnostics of Bureau & Athanassoula (2004), which directly probe the shape of the potential (but see also Bettoni & Galletta 1994; Kuijken & Merrifield 1995).

The importance of B/PS bulges goes beyond their sheer number and interesting morphology, as they may hold vital clues for our understanding of bulge formation. There is growing evidence against significant merger growth in many bulges (e.g. Kormendy 1993; Andredakis, Peletier, & Balcells 1995; MacArthur, Courteau, & Holtzman 2003; Balcells et al. 2003) and a corresponding emphasis on secular evolution processes, largely bar-driven (e.g. Wozniak et al. 1995; Erwin & Sparke 2002). Most theoretical models involve the growth of a central mass through bar inflow and/or possibly recurring bar destruction (e.g. Pfenniger & Norman 1990; Friedli & Benz 1993, 1995; Norman, Sellwood, & Hasan 1996), although the efficiency of bar dissolution mechanisms remains uncertain (Shen & Sellwood 2003 and references therein). Nevertheless, because of their probable relationship to bars, B/PS bulges are likely to play a central role in those scenarios, and a proper understanding of their structure and dynamics is essential to constrain them.

Our primary goal in this work is thus to study the stellar kinematics of a statistically significant number of galaxies with a B/PS bulge, simultaneously and independently verifying their relationship to bars and probing for embedded structures. We study Bureau & Freeman's (1999) sample of 23 edge-on spirals, 17 with a B/PS bulge and 6 with other bulge types, as well as an additional 7 B/PS bulges which showed little (or confined) emission and were only briefly discussed by the authors. The latter offer the best comparison with N-body models, being largely gas and dust free.

In § 2, the stellar kinematic bar diagnostics of Bureau & Athanassoula (1999) and Bureau & Athanassoula (2004) are summarized. In § 3, we describe the sample, observations, as

well as the reduction and analysis of the data. The stellar kinematics of the 30 galaxies is presented briefly in § 4, while § 5 discusses in greater detail the structure and dynamics of B/PS bulges and how they fit into bar-driven secular evolution scenarios. We summarize our results and conclude briefly in § 6.

2. Bar Diagnostics

As B/PS bulges are only visible in (quasi-)edge-on galaxies, a reliable morphological identification of bars is impossible. A plateau in the light distribution along the majoraxis has often been argued to trace bars (e.g. Wakamatsu & Hamabe 1984; de Carvalho & da Costa 1987; Lütticke et al. 2000b; but see also Bureau & Athanassoula 2004), but axisymmetric structures such as rings and lenses can also account for them. In fact, it is possible to construct axisymmetric B/PS bulges with simple two-integral distribution functions (Rowley 1988). We thus need bar identification methods for edge-on disks relying on kinematics, truly probing the shape of the galactic potential.

Adopting a generic barred galaxy mass model, Bureau & Athanassoula (1999) used periodic orbit families as building blocks to produce synthetic PVDs of barred galaxies seen edge-on. They showed that because of the non-homogeneous distribution of orbits in a barred disk, characteristic gaps occur in the PVDs between the signatures of the different orbit families. These can be used to kinematically identify an edge-on bar and constrain its viewing angle and mass distribution. Unfortunately, those models are too primitive to be compared with either the observed gas or stellar kinematics. The gas does not follow periodic orbits, being affected primarily by shocks and dissipation. This led Athanassoula & Bureau (1999) to develop more reliable gas kinematic diagnostics using the same mass model but full hydrodynamical simulations. These were successfully used by Bureau & Freeman (1999) in their ionized-gas study. Stars can also move on regular (quasi-periodic), irregular, and chaotic orbits and must of course form a self-consistent system, effectively smearing out the signatures predicted by Bureau & Athanassoula (1999). More refined stellar kinematic models are thus needed.

Bureau & Athanassoula (2004) developed fully self-consistent stellar kinematic bar diagnostics for edge-on disks using high-quality N-body simulations similar to those of Athanassoula & Misiriotis (2002) and Athanassoula (2003). The simulations include a luminous disk and a live dark halo, but no initial bulge component. For various viewing angles, (large) inclinations, and bar strengths, Bureau & Athanassoula (2004) extracted the stellar kinematics along a slit aligned with the photometric major-axis, contrasting the results with those of an axisymmetric disk. Like most observers, they parametrized the kinematics with a Gauss-Hermite series (see, e.g., van der Marel & Franx 1993; Gerhard 1993), using the same routine as used here (although no deconvolution is required in the N-body case; see § 3). The characteristic bar signatures observed are numerous: i) a major-axis light profile (I) with a quasi-exponential central peak and a plateau at moderate radii; ii) a "doublehump" rotation curve, that is a mean velocity (V) profile showing an initial rise followed by a plateau or slight decrease and a second rise to the flat part of the rotation curve; iii) a flat-top or weakly-peaked velocity dispersion (σ) profile with a secondary peak or plateau and, occasionally, a local central minimum (strong bars only); iv) an h_3 profile *correlated* with V over the projected bar length; and v) an h_4 profile with central and secondary minima. Throughout this paper, h_3 and h_4 represent respectively the asymmetric (skewness) and symmetric (kurtosis) deviations of the line-of-sight velocity distribution (LOSVD) from a pure Gaussian, while V and σ have their usual meanings (see § 3).

Those bar signatures are restricted to the projected bar length and are strongest when the bar is seen end-on, gradually weakening as the bar is viewed more side-on and they are stretched out (see Bureau & Athanassoula 2004). In other words, the plateaus in the light profile and the rotation curve, the peak in the dispersion, and the $h_3 - V$ correlation are all stronger when the bar is seen end-on. This is particularly useful as it is opposite from the morphological bias, whereby the characteristic peanut shape is seen for side-on projections and indiscriminate round shapes are seen end-on. As expected, the strengths of all the bar signatures also correlate with the strength of the bar itself (and the associated formation of an inner ring). Furthermore, while one can probably build axisymmetric configurations giving rise to the I, V, or σ signatures individually (e.g. double-disk structures), their radial extents are correlated (Bureau & Athanassoula 2004) and the behavior of h_3 appears characteristic of non-axisymmetric systems (although it is not uniquely related to them). Indeed, the LOSVDs of (inclined) axisymmetric systems will generally have a steep prograde wing and a tail of lower velocity material, yielding an anti-correlation of h_3 and V. For decreasing surface brightness profiles, non-axisymmetric motions thus appear required for h_3 and V to correlate.

In an ideal situation, one would like to use both morphological and kinematic information to study the intrinsic structure of a galaxy. In this paper, however, we will mainly rely on the aforementioned stellar kinematic diagnostics for V, σ , and h_3 . Our h_4 profiles generally have too low signal-to-noise ratios S/N to be of much use, and we defer discussion of the light profiles to a forthcoming pair of papers where high quality K-band observations will be presented (Aronica et al. 2004; Athanassoula, Aronica, & Bureau 2004).

3. Observations and Data Reduction

3.1. Sample

We use the sample of Bureau & Freeman (1999; see also Bureau 1998), consisting of 30 edge-on spiral galaxies selected from the catalogs of Jarvis (1986), Shaw (1987), and de Souza & dos Anjos (1987; disk galaxies with a B/PS bulge), and from that of Karachentsev, Karachentseva, & Parnovsky (1993; galaxies with extreme axial ratios). All objects are visible from the south ($\delta \leq 15^{\circ}$) and have bulges larger than 0.6 in diameter, to have enough spatial resolution to resolve the expected bar signatures with moderate seeing. In addition, for quick imaging with a small-field near-infrared (NIR) camera, we required $D_{25} \leq 7'$ (where D_{25} is the diameter at the 25 mag arcsec⁻² isophotal level in B).

General properties of the sample galaxies are summarized in Table 1. About threequarters of the galaxies either have probable companions or are part of a group or cluster, including a few with alignments apparently suitable for accretion (e.g. Binney & Petrou 1985). However, on the whole, the sample is not biased either against or for galaxies in a dense environment. Of the 30 galaxies, 24 were identified to have a B/PS bulge by Jarvis (1986), Shaw (1987), and de Souza & dos Anjos (1987). The other 6 galaxies were also selected from those catalogs but show more varied morphologies, mostly spheroidal. Those 6 objects thus constitutes a "control" sample for comparison. As we have already mentioned, however, N-body simulations indicate that a (thick) bar seen end-on will appear round, so we can expect some of the control sample galaxies to be barred as well. Indeed, in their study of the gas kinematics, Bureau & Freeman (1999) found weak bar signatures in 2 of the 6 control galaxies (NGC 3957 and NGC 4703).

Since the sample has been put together from several catalogs, the classification of the bulges' shapes is likely to be inhomogeneous. Fortunately, however, the more recent and larger survey of Lütticke et al. (2000a) includes all of our sample galaxies. Although their classification is somewhat subjective, relying on visual inspection of contour plots from galaxy images (like the other authors), Lütticke et al. (2000a) did apply a consistent judgment to the entire sample so their classification should at least be homogeneous. We compare in Table 2 the classification of Lütticke et al. (2000a) with that adopted by Bureau & Freeman (1999) from the catalogs of Jarvis (1986), Shaw (1987), and de Souza & dos Anjos (1987). A few galaxies absent from the latter catalogs were also classified by Bureau & Freeman (1999) themselves (PGC 44931, IC 5096, NGC 4703, and NGC 5084). The classifications are consistent for 85% of the galaxies. Three objects (NGC 1596, IC 5096, and ESO 240-G011) are classified as boxy by Bureau & Freeman (1999) but as ellipsoidal by Lütticke et al. (2000a), and one object the opposite (NGC 3957). Bar signatures were subsequently found

by Bureau & Freeman (1999) in both IC 5096 and ESO 240-G011.

The uncertainties related to the morphological identification of bars in edge-on systems through the presence of a B/PS bulge underscore the necessity of kinematic studies. Since all galaxies with extended ionized-gas emission were previously studied by Bureau & Freeman (1999), we will somewhat focus here on the 7 objects with little (or confined) emission. Those are all dust-free early-type spirals and should provide high quality stellar kinematics. The other galaxies are nevertheless important to confirm or infirm the kinematic bar detections of Bureau & Freeman (1999) and to study the effects of gas.

Although the classification of the bulges' shape is robust between the optical and NIR (e.g. Lütticke et al. 2000a), NIR images are essential to study their detailed structure because of significant extinction in most objects (e.g. Lütticke et al. 2000b). Clearly then, the observations from this paper should be reexamined in view of the K-band images to be presented in Aronica et al. (2004) and Athanassoula et al. (2004). Preliminary results have appeared in Aronica et al. (2003).

3.2. Observations and Data Reduction

Sets of long-slit spectroscopic observations were obtained along the major-axis of each sample galaxy with the Double Beam Spectrograph of the 2.3 m telescope at Siding Spring Observatory, Australia. The observations were carried out between 1995 December and 1997 May for 39 nights in total. The red and blue arms of the spectrograph each cover about 950 Å and were centered, respectively, on the H α λ 6563 line and the Mg b λ 5170 triplet for a redshift of 2000 km s⁻¹. Total exposure times ranged from 12 000 to 21 000 s per object, split into 1500 s exposures. When no emission line was detected within 3000 s, the red arm of the spectrograph was recentered on the Ca II λ 8600 triplet. 1752 × 532 SITE ST-D06A thinned CCDs were used for all observations. All galaxies were observed with a 1".8 × 400" slit. When a strong dust lane was present, the slit was moved just above the major-axis. We note however that the objects were acquired by visually aligning the nucleus and major-axis on the slit using a slit-viewing video camera. As the system was rather insensitive, the positioning of the slit was not very accurate, especially for low surface brightness objects.

Ionized-gas kinematics extracted from the red arm have already been presented and discussed by Bureau & Freeman (1999) for all objects with extended emission. Here we will focus on the blue arm data, best suited to study the stellar kinematics using the absorption lines of the Mg *b* triplet, H β λ 4861, and Fe. The dispersion was ≈ 0.55 Å pix⁻¹, yielding a 2-pixel spectral resolution of 64 km s⁻¹ ($\sigma_{inst} = 27$ km s⁻¹; see below). The spatial sampling

was $0^{\prime\prime}_{...9}$ pixel⁻¹ with typical seeings of $1^{\prime\prime}_{...0} - 1^{\prime\prime}_{...5}$.

All data were reduced using standard procedures in IRAF (Image Reduction and Analysis Facility). The (two-dimensional) spectra were first bias-subtracted using virtual overscan regions and bias frames, dark-subtracted (when necessary), and flat-fielded using flattened continuum lamp exposures. Each spectrum was then wavelength-calibrated using bracketing arc lamp exposures and the spectra were simultaneously rebinned to a logarithmic wavelength (linear velocity) scale, corresponding to about 32 km s⁻¹ pixel⁻¹ over the observed wavelength range (4760 - 5710 Å). The spectra were then corrected for vignetting along the slit using sky exposures. Every exposure was corrected for Earth's motion and relevant groups of exposures registered and combined. The resulting spectrum of each object was sky-subtracted using source-free regions along the slit and continuum normalized using a third-order spline with a small number of pieces. These two-dimensional spectra, from both galaxies and template stars, form the basis of the subsequent analysis aiming to extract the stellar kinematics.

Because only 3 template stars were observed systematically over the entire observing program, we selected the Fourier Correlation Quotient (FCQ) algorithm of Bender (1990) to derive the stellar kinematics of the galaxies. This method is based on the deconvolution of the peak of the template-galaxy correlation function with the peak of the template autocorrelation function and is relatively insensitive to template mismatch (see, e.g., van der Marel & Franx 1993). Furthermore, being recovered non-parametrically, the LOSVDs can be easily compared with those obtained from N-body simulations. We subsequently fitted the LOSVDs with a Gauss-Hermite series (van der Marel & Franx 1993; Gerhard 1993), yielding the mean stellar velocity V and the velocity dispersion σ , as well as the asymmetric (h_3) and symmetric (h_4) deviations from a pure Gaussian. This is essential given the complex shapes expected from the profiles (see Bureau & Athanassoula 2004). We nevertheless fit V and σ independently of h_3 and h_4 so that our results are directly comparable with single Gaussian fits. We use the deconvolution and fitting algorithms as originally implemented in the XSAURON software package (see Bacon et al. 2001; de Zeeuw et al. 2002).

The resulting stellar kinematics for the 30 sample galaxies are presented in Figure 1 (B/PS bulges with no or confined emission), Figure 2 (B/PS bulges with extended emission), and Figure 3 (control sample; all with extended emission). The latter two figures can be directly compared to those in Bureau & Freeman (1999) for the gas kinematics. From top to bottom, each panel shows an optical image of the galaxy (with isophotal contours) and registered V, σ , h_3 , and h_4 profiles along the major-axis. The spatial scale varies from galaxy to galaxy but the kinematic limits are the same. The data were folded under the assumption of bisymmetry and the errors reported are half the difference between the approaching and

receding sides of each galaxy. When the datum from one side is missing or corrupted (e.g. due to failure of the deconvolution algorithm or a foreground star), the datum is mirrored and denoted by a cross without an error bar. To ensure a homogeneous and minimal S/N in the outer parts of the galaxies, the data were binned until $S/N \ge 5$ per spatial and spectral element for V and σ and $S/N \ge 10$ for h_3 and h_4 , explaining the different bins for those quantities. The final S/N is thus at least $5 \times \sqrt{2} \approx 7$ for V and σ and $10 \times \sqrt{2} \approx 14$ for h_3 and h_4 .

3.3. Data Quality Tests

We tested our results for various sources of errors and uncertainties: strong sky emission lines, template mismatch, erroneous continuum normalization, variable spectral focus, and strong galactic emission lines.

A number of night sky emission lines from natural (e.g. N I, O I) and man-made (e.g. Hg I, Na I) sources are present in the observed wavelength range (see Massey & Foltz 2000). All were successfully removed by our sky subtraction algorithm except for the strongest O I telluric emission line at λ 5577, where the resulting artifacts are sufficient to affect our measurements, especially for faint galaxies. The spectra were thus truncated shortward of λ 5577, shortening the spectra by about 150 Å. This barely affects the quality of our measurements as there are no important galactic absorption lines longward of λ 5577 in our spectral range.

As gas kinematics was the primary goal of our observations, only two different types of stars were observed: K1 III (CPD -43°2527 and HD 176047) and G5 IV (HD 101266). This seriously limits our ability to quantify the effects of template mismatch, but the stellar kinematics of all the objects was nevertheless derived using both types of star and the results compared. As expected, no qualitative or significant quantitative differences were found, except for h_4 which is known to be particularly sensitive to mismatch (e.g. van der Marel & Franx 1993). Our h_4 profiles are in any case noisy and will not be discussed in any depth. The results presented throughout this paper were thus derived using a K1 III star only, and the effects of template mismatch will not be discussed further.

We also tested for the effects of imperfect continuum normalization by comparing the stellar kinematics obtained from good and bad normalizations of both galaxies and template stars. We used a linear fit to the continuum for bad normalizations and a cubic spline of order 8 for good normalizations (≈ 100 Å per order; our default value). We found that only a bad continuum normalization of the template stars affected our results. But since template

star spectra have high S/N and are few, obtaining a high quality continuum subtraction is both fast and easy. Continuum normalization is therefore not an issue for our data.

Although the instrumental setup was the same for all observing runs, a number of parameters such as the spectral focus (spectral resolution) were set manually and could have changed slightly from run to run. We checked for any effect by comparing the kinematics of galaxies observed over more than one run, and by deriving the kinematics of a few objects using template stars observed over different runs. No significant differences were found. A more worrying issue concerns the spectral resolution near the ends of the slit, as it was not always possible to obtain a uniform spectral focus over the entire slit length. In certain runs, judging from arc lamp exposures, the spectral resolution degraded significantly and the spectral point-spread-function (PSF) became non-Gaussian at the slit ends. Since template stars were only observed in the central parts of the slit, this could result in artificially high velocity dispersions and biased h_3 and h_4 measurements at large galactic radii. While we have no direct way of quantifying these effects (except for characterizing the widening of the arc lines themselves in arc lamp exposures), only a few galaxies have stellar measurements extending over a substantial portion of the slit, with 2 galaxies just reaching 50% (NGC 4710 and NGC 5746). Those do not show any peculiarities or systematic behavior at large radii, so we believe our measurements to be reliable over the radial range probed in all objects. In any case, our analysis will focus on the central regions of the galaxies only (within two bulge diameters), well within the properly focused region.

Lastly, we tested for possible effects due to the presence of galactic emission lines, which were not subtracted prior to deconvolution, and can not be masked when using FCQ. The emission line of [O III] $\lambda 5007$ is detected in most objects and that of H β (superposed on the corresponding absorption line) in about half, although both are rather weak in most cases. The [N I] $\lambda 5200$ doublet is not detected in any object, allowing us to compare the stellar kinematics obtained from a narrow range of wavelengths around the Mg b triplet (unaffected by emission lines) to that derived from the entire spectra. Using a short wavelength range is not advised with FCQ but does not appear problematic here. Using the same spatial bins, no significant difference is found for the odd moments of the velocity profiles (V and h_3), except for increased noise in the shorter spectra as expected (and the failure of the algorithm for ESO 151-G004 and ESO 597-G036, two of the three faintest galaxies). However, as shown in Figure 4, the σ profiles derived from the shorter unaffected spectra are systematically higher for about one-third of the objects (by typically 20 km s⁻¹ but up to 100 km s⁻¹). This occurs over a limited radial range, typically encompassing the rapidly rising part of the rotation curve and never extending past the first velocity plateau (see § 4). It could indicate that the kinematics of those objects is indeed affected by strong emission, since Bureau & Freeman (1999) identified numerous bright, rapidly rotating ionized-gas disks (nuclear spirals) in those regions. However, there is no direct relationship between the strength of the central emission and the differences in velocity dispersions, suggesting a more complex explanation. As we will argue later (see § 5.3), it is likely that the ionized-gas disks are associated with star formation and a dynamically cold, young population of stars. These would have little effect on the Mg *b* triplet but would strongly influence the H β line, biasing any measurement including the latter to lower values (as observed). This also suggests that a single late-type stellar template is not a sufficiently accurate representation of the effective stellar type of many sample galaxies over the entire radial range observed (although it usually does a fine job in the outer parts). Fortunately, however, the qualitative behavior of the profiles (on which our analysis relies) is not substantially affected.

3.4. Comparison with Published Data

Comparisons of our data with published stellar and gas kinematics are shown in Figures 5 and 6, respectively. We found only 5 galaxies with published stellar V and/or σ profiles (whether in tabular or figure formats): NGC 1381 (Dressler & Sandage 1983; D'Onofrio et al. 1995), NGC 2310 (Longo et al. 1994), NGC 128 (Dressler & Sandage 1983; D'Onofrio et al. 1995), NGC 5084 (Dressler & Sandage 1983), and NGC 5746 (Bower et al. 1993). See also Bertola & Capaccioli (1977) and Emsellem & Arsenault (1997) for NGC 128. 9 galaxies have available ionized-gas rotation curves, all of them measured from H α : IC 4767 (Rubin, Whitmore, & Ford 1988; Amram et al. 1995), NGC 1886, NGC 2788A, IC 2531, ESO 443-G042, ESO 240-G011 (Mathewson, Ford, & Buchhorn 1992), NGC 4469, NGC 4710 (Rubin, Waterman, & Kenney 1999), and ESO 597-G036 (Nishiura et al. 2000). We note that Bureau & Freeman (1999) did not extract rotation curves from their data, relying instead on the entire PVD diagrams. Although the identification of the approaching and receding sides in the literature is not always consistent with ours, we use matching sides here for comparison.

For the stellar kinematics, our data generally have better spatial sampling and systematically extend to larger radii than published data (see Fig. 5). NGC 1381 and NGC 128 are best suited for comparison since they have recent measurements also derived with FCQ (D'Onofrio et al. 1995). The agreement is excellent, except for NGC 1381 at large radii where our σ measurements are systematically lower. However, we believe that this is due to D'Onofrio et al.'s (1995) lower spectral resolution ($\sigma_{inst} \gtrsim 43 \text{ km s}^{-1}$ rather than 27 km s⁻¹ here) and we favor our results. The discrepancies in V for NGC 128 at large radii are not serious since the galaxy is disturbed at large radii and our data are folded. Bower et al.'s (1993) measurements of NGC 5746, obtained by cross-correlation (Tonry & Davis 1979), are also in good agreement, except for a few arcseconds at positive V (one-sided feature). In the

central 15", σ is in agreement with the values derived from Mg b only. Dressler & Sandage's (1983) data for NGC 1381, NGC 128, and NGC 5084 only marginally agree with our, but they are of much lower quality, have much lower spectral resolution ($\sigma_{\text{inst}} = 140 \text{ km s}^{-1}$), and were taken through a much wider slit. Our data should thus be considered superior. The only true problem lies with NGC 2310, where our measurements strongly disagree with literature data, also derived with FCQ but limited to the inner 5". We have no convincing explanation for the differences but offer a few hypotheses. Very bad seeing could explain our V and σ measurements, systematically lower than those of Longo et al. (1994), but the effect seems too large. Another possibility is that our slit was positioned slightly above (or below) the major-axis. As discussed above, positioning the slit with precision was difficult, but unless the vertical gradients of the mean velocity and velocity dispersion are very steep, the magnitude of the effect is unlikely to be sufficient. If NGC 2310 is indeed barred (see § 5), these gradients are expected to be shallow (see, e.g., Combes et al. 1990). Another possible explanation is that the error bars from Longo et al. (1994), which are not detailed but are of comparable sizes to those of the other galaxies studied, are underestimated. Indeed, NGC 2310 was observed with one of the shortest integration times (2700 s) and with the worst spectral resolution ($\sigma_{\rm inst} \gtrsim 142 \text{ km s}^{-1}$) of their entire sample, and the dispersions could be systematically overestimated.

The comparison with published gas kinematics is presented for reference only. The gas and stellar kinematics can not be easily compared, so any discrepancy between ours and published data can not be straightforwardly assigned to technical or reduction/analysis problems. In particular, the gaseous tracers used in Figure 6 most likely lie in a rotationally supported disk with small velocity dispersion, while stars can have significant pressure support and correspondingly reduced rotation, especially in the central parts. Furthermore, the gas can be strongly affected by shocks, inflow, etc (see Athanassoula & Bureau 1999). All these effects are indeed observed in Figure 6, where the agreement between our stellar measurements and published gas kinematics is always good in the outer parts but half the galaxies are discrepant in the central regions. In the galaxies where the effect is strongest (IC 4767, NGC 4469, NGC 4710, and NGC 5746), large B/PS bulges are present and Bureau & Freeman (1999) identified fast-rotating central gas components (nuclear spirals), apparently associated with x_2 -like streamlines (Athanassoula 1992a,b).

4. Results

4.1. Rotation curves and asymmetries

A look at Figures 1–3 quickly reveals that most galaxies with a B/PS bulges display a "double-hump" rotation curve, as expected from a barred disk (see § 2; Bureau & Athanassoula 2004). The most extreme examples are NGC 6771, NGC 128, and NGC 5746, where the V profile decreases significantly after a steep initial rise, before rising again slowly to the flat part of the rotation curve (the so-called turnover radius). Most galaxies, however, show a rather flat velocity plateau at intermediate radii (e.g. NGC 1596, IC 4767, and PGC 44931), while a few merely show a change of slope in the rising part of the rotation curve (e.g. NGC 4710, NGC 4469, and IC 5096). Only 3 of the 24 galaxies with a B/PS bulge show no evidence of a double-hump V profile: NGC 3390, ESO 443-G042, and ESO 240-G011. One could argue that this is also the case for NGC 1886 and IC 2531, but the latter (like ESO 443-G042) is heavily obscured by dust and the extracted kinematics is unreliable. Most galaxies of the control sample (4/6) show a featureless rotation curve smoothly rising in the inner parts, as expected for an axisymmetric object (e.g. Bureau & Athanassoula 2004). NGC 3957 and NGC 4703, however, do show a double-hump feature.

Since double-hump velocity profiles can equally be explained by carefully-constructed axisymmetric models (e.g. double-disk structures), the h_3 profiles are crucial to argue for triaxiality (Bureau & Athanassoula 2004). The quality of the h_3 profiles varies enormously across the sample, from excellent (e.g. NGC 1381, NGC 5746, and NGC 6722) to almost useless (e.g. NGC 1886, ESO 443-G042, and NGC 2788A). For essentially all B/PS bulges with an acceptable h_3 profile (arguably 20/21 galaxies), h_3 is correlated with V over a large radial range in the central parts, as expected from a projected barred disk (but contrary to expectations for an axisymmetric one; see $\S 2$ and Bureau & Athanassoula 2004). For most of those objects (17/20 galaxies), however, this correlation is not valid over the entire bulge region, but only roughly within the flat part of the rotation curve at moderate radii (the first V plateau). Most objects show an $h_3 - V$ anti-correlation over a short radial range in the very center, corresponding approximately to the rapidly rising part of the rotation curve. The best examples of this are NGC 1381, NGC 3203, NGC 128, and NGC 5746, while some of the weakest trends are seen in IC 4767, ESO 185-G053, and NGC 4469. Only 3 of 21 galaxies do not show this central anti-correlated component, and the h_3 profile of ESO 597-G036 is anti-correlated over its entire radial range. We note also that outside the range where h_3 is correlated with V (i.e. from the second rise in the rotation curve), h_3 and V are generally anti-correlated again. Two h_3 slope reversals are therefore the norm, and a third one is often seen in the outer disk (e.g. NGC 1596, NGC 3203, NGC 5746, and NGC 6722). Surprisingly, only 3 of the 6 galaxies in the control sample behave as expected for axisymmetric objects (NGC 1032, NGC 5084, and IC 5176). NGC 3957 and NGC 4703 are again bar-like, while NGC 7123 shows a region where h_3 may be correlated with V (although the profile is unreliable, most likely due to dust).

The V and h_3 trends are perhaps better illustrated in Figures 7 and 8, where the dimensionless parameter V/σ is shown as a function of the projected radius and h_3 is shown as a function of V/σ , respectively. The rise of V/σ is nearly linear with radius for all galaxies, although it flattens out in the outer parts for some. h_3 and V/σ are generally anti-correlated at small and large V/σ values (small and large radii), while they are correlated at moderate V/σ (moderate radii), where the bar is thought to dominate (see § 5). Figure 9 provides a schematized view of the V, σ , and h_3 profiles summarizing the trends observed in B/PS bulges.

We note that we have verified that the $h_3 - V$ (anti-)correlations can not be introduced by folding the data. If this was the case, the error bars as defined would clearly indicate it (e.g. they would always cross the $h_3 = 0$ line) and we would consider the (anti-)correlations insignificant. The same behavior is observed in the non-folded profiles, only at lower S/N.

4.2. Dispersions and symmetries

There is a great variety in the observed velocity dispersion profiles. A few galaxies possess a flat central σ peak with a broad shoulder and a small secondary peak (e.g. IC 4767 and ESO 185-G053). Most galaxies, however, have a sharper central peak with a gently decreasing shoulder, sometimes showing hints of a secondary maximum. Typical examples include NGC 1381, NGC 3203, and NGC 4469. N-body simulations predict both types of behavior, the former for stronger and the latter for weaker bars (see Athanassoula & Misiriotis 2002; Bureau & Athanassoula 2004). Yet other galaxies only show a dominant, broad central peak with a clear secondary peak (e.g. NGC 128, NGC 5746, and NGC 6722). The secondary dispersion maximum is usually strongest in the galaxies with a strong double-hump velocity profile (a presumably strong bar).

Many σ profiles also show a central depression, that is a more or less extended local central minimum. The best examples are NGC 5746, NGC 4469, and NGC 4710, where the depression extends over several arcseconds, but many galaxies show a central minimum in the central 1 – 2 pixels only (e.g. NGC 128, NGC 2788A, and NGC 5084). Similar local σ minima were observed in the N-body simulations of Bureau & Athanassoula (2004) but were generally restricted to the strongest bars, so we will discuss them at more length in § 5.2. In total, 10/24 galaxies with a B/PS bulge and 3/6 galaxies from the control sample have a clear local central σ minimum, while a few more have marginal signatures. This result is not affected by the spectral range used (whole spectra or Mg *b* region only; see Fig. 4) and is particularly surprising since local central σ minima are generally thought to be rare, although it may be due to dust in a few cases (e.g. NGC 2788A and NGC 7123). In the velocity dispersion profile compilation of Bottema (1993), only one clear example is present out of 12 intermediate-type spirals. On the other hand, a central σ minimum is visible in 7 of the 18 S0s studied by Fisher (1997), entirely consistent with our result. There, the minimum is only apparent along the minor-axis for 4 objects, suggesting that we would detect an even larger fraction of galaxies with a local central σ minimum if we had minor-axis profiles. Such a situation can easily arise if the kinematically cold component is more flattened than the spheroid (e.g. de Zeeuw et al. 2002; Emsellem et al. 2004). Recently, Emsellem et al. (2001) report a central σ minimum in 3 of 4 intermediate-type spirals studied, suggesting that the fraction increases as the quality (and most importantly the spatial resolution) of the data increases.

The h_4 profiles of the sample galaxies generally have low S/N and their measurement is somewhat affected by emission and template mismatch. We therefore refrain from a detailed discussion of their properties. Let us simply note that the inner parts of the profiles are generally correlated with σ (e.g. NGC 128 and NGC 5746), but that there are a few exceptions (e.g. NGC 1381 and ESO 240-G011). No correlation with the bulge shape or other kinematic quantities is apparent.

5. Discussion

5.1. B/PS Bulges and Bars

Our observations clearly show that most galaxies with a B/PS bulge display the stellar kinematic signatures expected from a barred disk seen edge-on (see § 2; Bureau & Athanassoula 2004). Indeed, as sketched in Figure 9, most galaxies in Figures 1 and 2 show i) a double-hump rotation curve, ii) a rather flat or slightly peaked velocity dispersion profile with a broad shoulder (or secondary maximum) and, occasionally, a local central minimum, and iii) an h_3 profile correlated with V over the expected bar length (the first hump of the rotation curve). These results are summarized in the last column of Table 2, where the sample galaxies are labeled as "bar", "bar?", or "no bar" if they show at least 2, only 1, or none of the above 3 kinematic bar signatures.

Although it holds true for all B/PS bulges, the link with bars is clearest for the sample of galaxies with no (or confined) emission (Fig. 1), as well as for the earliest type galaxies in the second B/PS bulge sample (the S0s of Fig. 2), where the emission is very weak outside of the central ionized-gas disk (the nuclear spiral; see Bureau & Freeman 1999). Except for ESO 597-G036, which is strongly interacting, those galaxies systematically show all 3 kinematic bar signatures. Furthermore, the bulges' morphology does seem to correlate with the shape of the kinematic profiles (and thus the bar viewing angle) as expected (see § 2; Bureau & Athanassoula 2004). The strongest peanut-shaped bulges (e.g. IC 4767 and ESO 185-G053) show an extended first velocity hump (relative to the bulge size), a rather flat σ profile, and small h_3 amplitudes; rounder bulges (e.g. NGC 1381 and NGC 1596) have comparatively shorter velocity plateaus, more peaked σ profiles, and strong h_3 signatures. Furthermore, the galaxies with the strongest velocity plateaus (or dips) generally show the best evidence for a secondary dispersion peak (e.g. NGC 128 and NGC 6771).

Those morphology-viewing angle correlations are not in prefect agreement with the simulations' predictions, however, especially for galaxies with extended emission. Many peanut-shaped bulges show strong V double-humps, peaked σ profiles, and clear $h_3 - V$ correlations, in accordance with the presence of a bar but contrary to the viewing angle (or morphology) expectations (Bureau & Athanassoula 2004). This is best illustrated by NGC 128, NGC 5746, and NGC 6771, but see also NGC 6722, PGC 44931, and NGC 2788A. This suggests that the relationship between bulge morphology and bar viewing angle is not as straightforward as the N-body simulations suggest (e.g. Combes et al. 1990; Raha et al. 1991), or that the pure N-body kinematics is too idealized, particularly for gas-rich galaxies. The structure and dynamics of (thick) bars may be strongly influenced by the presence of a gas disk, as has been advocated by Berentzen et al. (1998). While they argued that the bar and buckling instabilities (and thus the boxiness of the bulges) are weakened by gas, which does not seem to be the case here (there are plenty of gas-rich but strong B/PS bulges), it would be interesting to see if the kinematic bar signatures are strongly affected.

Lessening the discrepancy between simulations and observations for the later type galaxies is the fact that the kinematic bar signatures are modified for non edge-on systems, as the line-of-sight integration through the outer parts of the disk decreases (see Bureau & Athanassoula 2004). For those cases, the V and h_3 signatures become more extreme and the secondary σ peak increases, particularly for side-on bar orientations. As the gas-poor early-type galaxies of the sample are perfectly edge-on, while the gas-rich late-type galaxies are generally less inclined (to avoid the dust lane), the latter are expected to have stronger signatures (in a relative sense). There does not seem to be an obvious correlation between inclination and bar signature strength, but the effects of dust are hard to quantify and some of the strongest bar signatures are indeed seen in non edge-on systems. The effect is thus likely present, but it is unclear whether it can account for the very strong bar signatures observed in objects such as NGC 5746 and NGC 6722. The complexity of the kinematic profiles can also be artificially increased by the presence of dust along the line-of-sight. The kinematics of a few galaxies with perfectly edge-on and strong dust lanes is probably unreliable (e.g. IC 2531 and ESO 443-G042) and other galaxies are likely to be affected to various degrees (e.g. NGC 2788A and IC 4937). The apparent shape of the bulges may also be modified, although their classification as B/PS bulges is probably unaffected (Lütticke et al. 2000b). To alleviate the extinction problem, we have acquired K-band imaging of all sample galaxies. A separate study of their morphology will appear in Aronica et al. (2004) and Athanassoula et al. (2004), and the gas and stellar kinematics of the sample shall be reexamined in light of those results. K-band images will be especially useful to constrain the scales over which the kinematic bar signatures occur. Currently, the extent of the features in V, σ , and h_3 can be compared among themselves, but they can only be roughly related to the relevant photometric scales of the bulge and disk.

To summarize, despite kinematic profiles in appearance more complex than those predicted by N-body simulations, our observations convincingly show that most galaxies with a B/PS bulge have a barred disk. This is because most galaxies possess the V, σ , and particularly the h_3 signatures expected from an edge-on bar (§ 2 and Bureau & Athanassoula 2004). This in turn strongly supports the suggestion that B/PS bulges are truly thick bars seen edge-on, although we have not probed the galaxies' potential out of the disk plane. Kinematics at large galactic heights is required for the latter, and we have acquired data for a few objects (Zamojski et al. 2004, in preparation).

As noted in § 1, some off-plane kinematic observations of B/PS bulges do exist in the literature (e.g. Bertola & Capaccioli 1977; Kormendy & Illingworth 1982; Rowley 1986; Jarvis 1987; Shaw 1993a; Shaw et al. 1993), but those were mostly concerned with the presence of cylindrical rotation rather than the current bar signatures. Cylindrical rotation is a generic prediction of (thick) bar models (e.g. Combes et al. 1990), but it is also consistent with axisymmetry (Rowley 1988).

Interestingly, the galaxies in the control sample do not systematically show the behavior expected for a simple axisymmetric disk: i) a smoothly rising rotation curve, ii) a monotonically decreasing velocity dispersion profile, and iii) an h_3 profile anti-correlated with V(see Bureau & Athanassoula 2004). Some of those galaxies may well have substructures, but the problem most likely arises from the heterogeneous nature of the control sample. Indeed, while there are a few catalogs of galaxies with a B/PS bulge (see § 3.1), there is no such thing for edge-on round bulges. The control sample was thus selected from the catalog of high axial ratio galaxies by Karachentsev et al. (1993) and from galaxies apparently misclassified in B/PS bulge catalogs. This is less than satisfying, and NGC 3957 and NGC 4703 clearly represent transition objects (weak B/PS bulges and thus probably weak bars). Those 2 objects have the "boxiest" bulges of the control sample and show characteristic kinematic bar signatures. Bureau & Freeman (1999) already pointed out that they have weak bar signatures in their ionized-gas kinematics. To confirm that most non-B/PS bulges are also non-barred (but not all, since some are expected to be if the bar is seen end-on), a study similar to ours but focusing instead on round bulges would be highly valuable. A larger and better defined control sample is thus essential to strengthen our results.

5.2. Inner Disks

As mentioned above, at least 10 of the 24 galaxies with a B/PS bulge ($\gtrsim 40\%$) show a decrease of σ in the very center. In a few galaxies, this local minimum extends over several arcseconds and can reach 15 – 20% of the observed peak (e.g. NGC 5746, NGC 4469, and NGC 4710), although it is generally much smaller in both size and intensity (e.g. NGC 128 and NGC 2788A). 8 of those galaxies also show a characteristic double-hump velocity profile. The standard explanation for both features is the presence of a cold central stellar disk originating from gas inflow (e.g. Emsellem et al. 2001). However, Athanassoula & Misiriotis (2002) noted the existence of central σ minima in purely dissipationless N-body simulations. Bureau & Athanassoula (2004) later showed that they can arise naturally from the orbital structure of (strongly) barred disks (depending on the axial ratio radial dependence of the x_1 orbits). We have so far argued for the latter possibility in this paper because of the $h_3 - V$ correlation at moderate radii (i.e. over the expected bar length), which is characteristic of triaxiality and bypasses the need for gas (Bureau & Athanassoula 2004).

However, the observations do show a strong anti-correlation of h_3 and V in the inner parts of most sample galaxies (including all those with a central σ minimum and a reliable h_3 profile; e.g. NGC 5746, NGC 4469, and NGC 128). This behavior is not observed in any of the N-body simulations of Bureau & Athanassoula (2004) and suggests that not only are the inner parts of the galaxies cold (i.e. rapidly rotating), but also that they are very close to axisymmetric. In those objects, the region where h_3 and V anti-correlate appears to have largely decoupled from the rest of the galaxy (and the bar) and circularized, forming a dense and (quasi-)axisymmetric central stellar disk. This is supported by the sharp transition between the $h_3 - V$ anti-correlation and correlation regions. Furthermore, (quasi-)axisymmetric central stellar disks naturally explain why prominent double-hump V profiles and central σ minima are observed in peanut-shaped bulges as well as boxy-shaped ones, contrary to viewing angle expectations. Once circularized, the kinematic signatures of the inner regions will be largely independent of viewing angle (but not exactly, because of the line-of-sight integration through the main disk, which remains non-axisymmetric).

As expected, the extent of the central $h_3 - V$ anti-correlation is roughly equal to that of the rapidly rising part of the rotation curve. If present, the extent of the central σ minimum is also equal or smaller (see Fig. 9; NGC 5746, NGC 4469, and NGC 4710). Of the 3 galaxies in the control sample which show a central σ depression, NGC 7123 is probably affected by dust, but NGC 5084 and IC 5176 appear as regular objects with large-scale axisymmetric disks (and no $h_3 - V$ correlation).

As our kinematic profiles are luminosity-weighted, the central disks could in principle be fairly bright but only marginally colder than their surroundings, or both much fainter and colder. The strong $h_3 - V$ anti-correlation argues that they are much colder. In either case, the luminosity requirement is most easily fulfilled for our sample as the (projected) surface brightness of disks is maximized when viewed edge-on (assuming the central disks to be coplanar with the large-scale galactic disks). A quantitative estimate of how luminous (and massive) these disks must be would nevertheless be useful, and the K-band images will help constrain this.

While the conventional view is that both a classical bulge and a (separate) bar can usually be clearly identified photometrically in face-on barred systems (at least in early-type ones), it is questionable whether those bulges are systematically hot. Arguments that central disks can masquerade as bulges date back at least to Kormendy (1982), and Kormendy (1993) reviewed much of the photometric and kinematic evidence available then. Among others, Seifert & Scorza (1996) and Erwin et al. (2003) more recently argued for the presence of significant central disks in bulges, using high-quality observations. In fact, much recent work shows that bulges are often not prominent and can have rather shallow light profiles, with Sersic index n ranging from roughly 0.5 to 2.5 (e.g. Andredaki et al. 1995; de Jong 1996; MacArthur et al. 2003; Balcells et al. 2003), as well as young stars and bar or spiral structures (e.g. Carollo et al. 1997, 1998; Erwin & Sparke 2002, 2003). See Kormendy (2001) for similar arguments.

Those observations raise the interesting possibility that the decoupled central stellar disks identified in most of the sample galaxies are in fact the so-called bulges seen in face-on barred galaxies. While their scale seems rather small (i.e. typically equal to the width of the bar), they are (quasi-)axisymmetric, have similar stellar kinematics, and also appear to have similar luminosity profiles. Indeed, even simple optical light profiles derived by summing our data in wavelength (not shown) show that the central light peak is close to exponential and typically extends over the first velocity hump only (approximately to the radius where the box/peanut shape is maximum, although this varies somewhat as a function of viewing angle). This again argues against merger-driven growth for those bulges and suggests that many classical bulges may well be concentrated disks (i.e. non-exponential disks), with a structure closer to truncated cylinders rather than spheroids (see Kormendy 1993). Axisymmetric "bulges" would then grow at the center of bars, rather than out of their destruction.

The implications from the above is that the central peak in the light profile, normally associated with the bulge in face-on systems, is kinematically cold and contained within the vertically extended (thick) region of edge-on systems (i.e. the B/PS bulge), itself only a portion of the bar (which extends to the turnover radius of the rotation curve). This clearly remains speculative without good quality photometry, but those issues will be explored further with the K-band observations presented in Aronica et al. (2004) and Athanassoula et al. (2004). Similar ideas are expressed by Erwin et al. (2003) in the specific cases of NGC 2787 and NGC 3945.

5.3. Secular Evolution

The N-body simulations discussed by Bureau & Athanassoula (2004; but see also Athanassoula 2002, 2003) undergo substantial bar-driven evolution as the disk transfers angular momentum to the halo. The bar and its associated kinematic signatures grow in length and strength with time, but there is no evidence that the central parts circularize. It is thus doubtful whether purely stellar processes could give rise to the central $h_3 - V$ anti-correlations and the (quasi-)axisymmetric central stellar disks argued for above.

On the other hand, our results fit nicely in a scenario where the identified central stellar disks form through bar-driven gas inflow. Because of the torques and shocks they generate, bars are very efficient at driving gas toward their centers (assuming there is a sufficient reservoir of material at large radii; see e.g. Athanassoula 1992b; Friedli & Benz 1993, 1995). The gas tends to accumulate near the inner Lindblad resonance (ILR, if present), often vigorously forming stars and giving rise to a highly visible nuclear ring (e.g. Wozniak et al. 1995; Martinet & Friedli 1997). The conditions and behavior of the gas at and within the ILR are still under debate (but see, e.g., Englmaier & Shlosman 2000; Shlosman & Heller 2002 and references therein), but this is unimportant for our discussion as long as a sufficient mass is accumulated to circularize the potential.

Once the potential is (quasi-)axisymmetric, h_3 and V will anti-correlate (but the V and σ signatures will persist). Furthermore, any star formation in the gas disk will enhance the stellar kinematic features and keep the central stellar disk cold, negating the effects of possible heating mechanisms. This is likely as there is overwhelming evidence for star forming central

loosely correlates with the strength of the central $h_3 - V$ anti-correlation. For the galaxies with no emission, we must assume either that the gas is not ionized or, more likely, that the reservoir of material has been exhausted and star formation in the central disks has ceased. This is consistent with the fact that no central σ minimum is seen in any of the gas-poor galaxies, suggesting that their central disks are kinematically hotter, and thus presumably older, than gas-rich systems (IC 4767 has strong emission but it is confined to the inner few arcseconds).

Current or recent star formation in the central disks is further supported by our experimentations with emission line subtraction (§ 3.3). Indeed, while the results for the two stellar templates (K1 III and G5 IV) are identical, this is not the case when using a single template and comparing the kinematics derived from the entire spectra (including H β) or the Mg *b* region only. Then, the *V* and h_3 profiles are essentially identical, but as shown by Figure 4 the Mg *b* dispersions are systematically higher for about one-third of the sample. As young stars contribute preferentially to H β , the older stars appear kinematically hotter. The effect extends mainly over the rapidly rising part of the rotation curve (or at most to the end of the first plateau), where the central σ minima and the $h_3 - V$ anti-correlations are observed. As the first velocity hump is originally caused by the projection of the x_1 orbits (perceived excess rotation; see Bureau & Athanassoula 2004), this implies that the central disks are always contained within the width of the bar, exactly what is expected if they are fed from it (shocks occur along the leading edges of the bar; see e.g. Athanassoula 1992b).

Our data thus seem perfectly consistent with a scenario where bars give rise to both the observed B/PS bulges (through bar-buckling) and decoupled, nearly axisymmetric central stellar disks (through gas inflow and subsequent star formation). Adding gas and star formation to the simulations of Bureau & Athanassoula (2004) or a detailed comparison with similar existing models (e.g. Heller & Shlosman 1994; Friedli & Benz 1995) would thus be extremely valuable. Given that at least 40-45% of bulges across all morphological types are B/PS (Lütticke et al. 2000a), our results have important implications for our understanding of the structure and evolution of all bulges. Bulges here appear to be made up mostly of disk material which has acquired a large vertical extent through vertical instabilities. Together with the central disks, they are thus consistent with a formation dominated by bar-driven secular evolution processes rather than merging.

We note however that while bar-driven secular evolution scenarios are often invoked to argue for a gradual drift of late-type bulges toward earlier types, this aspect of the scenarios is not effectively probed here. We have no way to tell whether the bars detected here will later on be destroyed by the sufficient accumulation of gas in their centers (e.g. Heller & Shlosman 1996; Norman et al. 1996 and references therein), thus contributing to the growth of a more axisymmetric spheroidal bulge, or whether this process may have already occurred in some of the galaxies. The kinematics presented here, although limited to the equatorial plane, appears perfectly consistent with that expected from disk material only. We do not *require* the presence of an additional "classical" (i.e. both axisymmetric and hot) bulge in addition to the (thick) bar detected. Whether we can rule out the presence of a rounder and more pressure supported component with our observations is harder to answer, and it would presumably require detailed modeling of individual objects. Such a component may be consistent with the velocity dispersion peaks observed in some objects (particularly when using Mg b only), but it tends to disagree with the flat σ profiles (or local central σ minimum) observed in others. K-band imaging and kinematics at large galactic heights are better suited to constrain the additional presence of a classical bulge and will be discussed elsewhere (Aronica et al. 2004; Athanassoula et al. 2004; Zamojski et al. 2004, in preparation). We note however that Erwin et al. (2003) argued for the presence of both a concentrated inner disk and a (much) smaller classical bulge in the two galaxies they studied (NGC 2787 and NGC 3945).

We also note that there is limited evidence from our sample for so-called hybrid bar/bulge formation scenarios (Mihos et al. 1995), whereby a bar is first excited by an interaction (e.g. Noguchi 1987; Gerin, Combes, & Athanassoula 1990) and then buckles. Indeed, NGC 128, NGC 6771, and ESO 597-G036 all have strong peanut-shaped bulges (strong bars) and presumably interacting close-by companions. Furthermore, NGC 128, NGC 1596, and NGC 3203 have counterrotating ionized-gas disks (Bureau & Chung 2004, in preparation), clear evidence for the accretion of external material.

5.4. Literature Data

A number of studies are now available in the literature containing extended and reliable stellar kinematic profiles of galaxies (many including h_3 and h_4). While they generally focus on early-type systems, we review below studies including a large number spirals and/or lenticulars, preferably viewed edge-on.

Fisher (1997) presents high quality stellar kinematic of 18 S0s. 9 are exactly or approximately edge-on, 6 of which appear boxy on the isophotes presented (NGC 1461, NGC 2560, NGC 4026, NGC 4036, NGC 4111, and NGC 4251). All of those show the characteristic kinematic bar signatures seen in the current sample (§ 2 and Bureau & Athanassoula 2004): double-hump rotation curve, velocity dispersion profile with a flat top and/or shoulder (or

secondary maximum), and h_3-V correlation at moderate radii. Two of the non-boxy galaxies show kinematic bar signatures (NGC 4350 and NGC 4762), but they also show photometric evidence of a bar (a plateau in the major-axis surface brightness profile at moderate radii; see Lütticke et al. 2000b and Bureau & Athanassoula 2004). They thus most likely harbor a bar seen end-on (but see Wozniak 1994 for NGC 4762). The third non-boxy galaxy (NGC 5666) shows neither kinematic nor photometric bar signatures. All the presumably barred galaxies also show an $h_3 - V$ anti-correlation in the center, as observed here. Fisher's (1997) results are thus entirely consistent and supportive of ours. Based on photometric evidence, he in fact suggested that bars could be at the origin of the h_3 slope reversals observed, but he lacked the diagnostics of Bureau & Athanassoula (2004) to confirm it. 3 of the above galaxies also show a central ionized-gas disk and 3 a local minimum in the minor-axis σ profile, further supporting the presence of a thin, rapidly rotating stellar (and sometimes gas) disk at the center of the objects. It would be interesting to see if the ionized-gas kinematics shows the same kind of bar signatures predicted by Athanassoula & Bureau (1999) and observed by Merrifield & Kuijken (1999) and Bureau & Freeman (1999).

Although we prefer to delay the discussion of photometric papers to Aronica et al. (2004), Seifert & Scorza (1996) discuss the photometry of 16 nearly edge-on S0s along with the stellar kinematics of 10. They derive the major-axis disk profile of each object by subtracting a pure ellipsoidal model constrained above the equatorial plane. They almost systematically identify an outer disk with an inner cut-off, but also a number of steep inner disks. Although no explanation is offered for either structure, those results are expected in the context of bar-driven secular evolution scenarios. 12 galaxies have a light profile plateau at intermediate radii, typical of a bar viewed edge-on. All the double-disks are observed in galaxies with such a plateau (i.e. a bar), as are all the rings identified. The latter also systematically occur at the end of the plateau and the turnover in the rotation curve, as expected for inner rings and bars (e.g. Bureau & Athanassoula 2004). Among the 8 objects with a light plateau and stellar kinematics (NGC 2549, NGC 2732, NGC 3098, NGC 4026, NGC 4111, NGC 5308, NGC 5422, and NGC 7332), 6 have a double-hump velocity profile characteristic of bars (all also have a double-disk structure) and only 2 do not (none have a double-disk structure). Given the poor spatial sampling of the data and the absence of error bars or seeing measurements, this is perfectly consistent with a one-to-one relationship between bars and light plateaus. Therefore, while Seifert & Scorza's (1996) inner disks can be assimilated with the central stellar disks argued for here (i.e. the central region where h_3 and V anti-correlate), their arguments for truncated outer disks are questionable. As one moves from the outside in, we see no evidence of a disk truncation, but rather simply the beginning of the bar and an increase in the scaleheight of the disk (the B/PS bulge and $h_3 - V$ correlation region; see Athanassoula et al. 2004). No separate (classical) bulge component is required either.

Emsellem et al. (2001) recently obtained high spatial resolution stellar kinematics of 4 intermediate-type barred spiral galaxies, each with a Seyfert nucleus, secondary bar, and moderate inclination (NGC 1097, NGC 1365, NGC 1808, and NGC 5728). All 4 galaxies show a double-hump rotation curve and 3 a central σ minimum. Simple dynamical models require the presence of decoupled central (and weakly non-axisymmetric) stellar disks, presumably fueled by bar-driven gas inflow and star formation. This scenario is identical to the one proposed here. Interestingly, the central disks required have similar masses and radii to the small (classical) spheroidal bulges assumed.

It would also be interesting to know if the so-called "double-wave" rotation curves, reported by Bettoni (1989) along the bar of many SB0s (7 of the 10 objects studied), could be related to the double-hump velocity profiles observed here (or to the presence of decoupled centers). A generic interpretation is harder in this case as the orientation of each object differs (orientation of the bar with respect to the line-of-nodes and inclination), but an explanation relying on the axial ratio variation of the x_1 orbits again appears likely (comparing to the 2D model of Sparke & Sellwood 1987; see also Bureau & Athanassoula 1999, 2004). A comparison with current 3D N-body simulations would be straightforward.

Going beyond kinematics, stellar populations also offer an important tool to constrain galaxy formation scenarios. The absence of correlations between velocity dispersion and linestrength gradients (at least in some bulge samples; e.g. Fisher, Franx, & Illingworth 1996; Fisher 1997) argues against pure dissipational collapse (Larson 1976; Carlberg 1984) and other arguments limit the influence of accretion and/or merging. Unfortunately, detailed predictions for the stellar populations are still largely inexistent for bar-driven secular evolution scenarios. Naively, one would expect bars to smooth out population gradients due to substantial radial (and vertical) motions, but any central star formation and subsequent stellar migration (mixing) will greatly complicate this picture and may actually enhance gradients in the center (for early models, see Friedli, Benz, & Kennicutt 1994; Friedli & Benz 1995). This seems to be borne out by observations (see, e.g., Martin & Roy 1994 and Zaritsky, Kennicutt, & Huchra 1994 for the gas; Fisher et al. 1996 for the stars), and NGC 4594 (Sombrero galaxy; Emsellem et al. 1996) and NGC 7332 (Falcón-Barroso et al. 2004) offer excellent examples where largely successful attempts have been made to interpret both the gaseous/stellar kinematics and the stellar populations coherently within a bar-driven secular evolution scenario. Nevertheless, detailed chemo-dynamical models of barred galaxies taking into account all of the above effects are urgently needed.

Integral-field spectrographs with a large field-of-view and sufficient wavelength coverage offer the best potential to constrain the intermediate-scale structure of galaxies and (in)validate formation scenarios. In this respect, the SAURON survey is particularly relevant, having mapped the ionized-gas distribution and kinematics, the stellar kinematics, and the linestrength indices (age and metallicity) of over 70 ellipticals, lenticulars, and Sa bulges to one effective radius (see de Zeeuw et al. 2002; Emsellem et al. 2004). The 2D information confirms that a number of galaxies possess a structure similar to that argued for here, i.e. a cold and thin central stellar disk (first V increment, central σ minimum, and $h_3 - V$ anticorrelation) embedded in a much larger and thicker triaxial component (first V plateau and $h_3 - V$ correlation). Central ionized-gas disks are also often cospatial with the central stellar disks. The best examples are NGC 4526 and NGC 3623 (de Zeeuw et al. 2002; Bureau et al. 2002a,b), but there are numerous others (Falcón-Barroso et al. 2004; Emsellem et al. 2004).

6. Conclusions

The (projected) morphology of B/PS bulges departs strongly from that of classical, spheroidal bulges (e.g. Shaw 1993b), implying an even more distorted 3D structure, but their high incidence ($\geq 45\%$ of all bulges; see Lütticke et al. 2000a) makes them more than simple curiosities and a widespread mechanism must be able to account for their structure and dynamics. By studying the stellar kinematics of the 30 edge-on spiral galaxies of Bureau & Freeman (1999), we have attempted here to discriminate between the two leading formations scenarios: accretion (e.g. Binney & Petrou 1985; Rowley 1988) and bar-buckling (e.g. Combes & Sanders 1981; Combes et al. 1990). The latter is particularly attractive in view of currently popular secular evolution scenarios, which argue that bars may drive bulges along the Hubble sequence (e.g. Friedli & Benz 1995; Norman et al. 1996 and references therein).

Our results are summarized in Table 2. 22 of 24 galaxies with a B/PS bulge show clear kinematic bar signatures ($\approx 90\%$), while only 2 of the 6 control sample galaxies do and are probably transition objects. We thus confirm the results of Bureau & Freeman (1999) for galaxies with extended ionized-gas and, for the first time, extend those results to gas-poor B/PS bulges (S0s). The kinematic evidence in favor of a close relationship between thickened bars and B/PS bulges is thus now overwhelming across all morphological types (S0–Sbc), although we still have not probed the potentials out of the equatorial plane. Zamojski et al. (2004, in preparation) shall discuss the stellar kinematics of a few objects at large galactic heights.

Most objects show kinematic profiles in agreement with those predicted from N-body simulations of barred disks (Bureau & Athanassoula 2004), including the expected relationship between bulge morphology and bar viewing angle. In particular, most galaxies with a B/PS bulge have i) a double-hump rotation curve with a dip or plateau at moderate radii, ii) a rather flat central velocity dispersion profile with a secondary peak or plateau and (in about 40% of cases) a local central minimum, and iii) an h_3 profile correlated with V over the expected bar length, with up to three slope reversals. As expected if caused by a bar, the strengths and extents of those features are correlated. Our h_4 profiles are generally too noisy to be of much use.

A number of differences with the simulations also exist, most of which appear related to the past or current presence of gas. In particular, the kinematic profiles of most galaxies show an anti-correlation of V and h_3 in the very center, over a region corresponding to the rapidly rising part of the rotation curve (or at most the first plateau) and encompassing the central light peak and central σ minimum (if present). Being cospatial with observed ionized-gas disks in gas-rich galaxies (Bureau & Freeman 1999), this kinematic behavior is most likely due to cold quasi-axisymmetric central stellar disks, which we argue have decoupled due to bar-driven gas inflow, and may have been enhanced by subsequent star formation. B/PS bulges are thus entirely consistent with the predictions of most bar-driven secular evolution scenarios (e.g. Heller & Shlosman 1994; Friedli & Benz 1995), whereby bars can simultaneously account for the creation of a large vertically extended component out of disk material and for the accumulation of mass in their centers (possibly associated with the so-called bulges of face-on systems), bypassing the need for merging or accretion of external material.

Lastly, we reiterate that h_3 is a very useful tracer of the structure and dynamics of galaxies. As suggested by Bureau & Athanassoula (2004), the correlation or anti-correlation of h_3 and V appears to be a reliable diagnostics of the intrinsic shape, at least for highly inclined disks.

Support for this work was provided by NSF grant AST 00-98249 to Columbia University and by NASA through Hubble Fellowship grant HST-HF-01136.01 awarded by the Space Telescope Science Institute, which is operated by the Association of Universities for Research in Astronomy, Inc., for NASA, under contract NAS 5-26555. M.B. wishes to thank K. C. Freeman for his involvement in the early stages of this project and E. Athanassoula, A. Bosma, and E. Emsellem for useful discussions. The Digitized Sky Surveys were produced at the Space Telescope Science Institute under U.S. Government grant NAG W-2166. The images of these surveys are based on photographic data obtained using the Oschin Schmidt Telescope on Palomar Mountain and the UK Schmidt Telescope. The plates were processed into the present compressed digital form with the permission of these institutions. This research has made use of NASA's Astrophysics Data System (ADS) Bibliographic Services and the Lyon-Meudon Extragalactic Database (LEDA; http://leda.univ-lyon1.fr).

REFERENCES

- Amram, P., Boulesteix, J., Marcelin, M., Balkowski, C., Cayatte, V., & Sullivan, W. T. 1995, A&AS, 113, 35
- Andredakis, Y. C., Peletier, R. F., & Balcells, M. 1995, MNRAS, 275, 874
- Aronica, G., Athanassoula, E., Bureau, M., Bosma, A., Dettmar, R.-J., Vergani, D., & Pohlen, M. 2003, in The Evolution of Galaxies III: From Simple Approaches to Self-Consistent Models, Ap&SS, 284, 753
- Aronica, G., Bureau, M., Athanassoula, E., Bosma, A., Dettmar, R.-J., & Freeman, K. C. 2004, MNRAS, submitted.
- Athanassoula, E. 1992, MNRAS, 259, 328
- Athanassoula, E. 1992, MNRAS, 259, 345
- Athanassoula, E. 2002, ApJ, 569, 83
- Athanassoula, E. 2003, MNRAS, 341, 1179
- Athanassoula, E., Aronica, G., & Bureau, M. 2004, MNRAS, submitted.
- Athanassoula, E., & Bureau, M. 1999, ApJ, 522, 699
- Athanassoula, E., & Misiriotis, A. 2002, MNRAS, 330, 35
- Bacon, R., et al. 2001, MNRAS, 326, 23
- Balcells, M., Graham, A. W., Dominguez-Palmero, L., & Peletier, R. F. 2003, ApJ, 582, 79
- Bender, R. 1990, A&A, 229, 441
- Berentzen, I., Heller, C. H., Shlosman, I., Fricke, K. J. 1998, MNRAS, 300, 49
- Bertola, F., & Capaccioli, M. 1977, ApJ, 211, 697
- Bettoni, D. 1989, AJ, 97, 79
- Bettoni, D., & Galletta, G. 1994, A&A, 281, 1
- Binney, J., & Petrou, M. 1985, MNRAS, 214, 449
- Bottema, R. 1993, A&A, 275, 16

- Bower, G. A., Richstone, D. O., Bothun, G. D., & Heckman, T. M. 1993, ApJ, 402, 76
- Bureau, M. 1998, Ph.D. Thesis, Australian National University
- Bureau, M., & Athanassoula, E. 1999, ApJ, 522, 686
- Bureau, M., & Athanassoula, E. 2004, ApJ, submitted.
- Bureau, M., et al. 2002a, in Galaxies: The Third Dimension, eds. M. Rosado, L. Binette, & L. Arias (ASP: San Francisco), 208
- Bureau, M., et al. 2002b, in The Dynamics, Structure & History of Galaxies, eds. G. S. Da Costa & H. Jerjen (San Francisco: ASP), 53
- Bureau, M., & Freeman, K. C. 1999, AJ, 118, 126
- Carlberg, R. G. 1984, ApJ, 286, 403
- Carollo, C. M., Stiavelli, M., de Zeeuw, P. T., & Mack, J. 1997, AJ, 114, 2366
- Carollo, C. M., Stiavelli, M., & Mack, J. 1998, AJ, 116, 68
- Combes, F., Debbasch, F., Friedli, D., & Pfenniger, D. 1990, A&A, 233, 82
- Combes, F., & Sanders, R. H. 1981, A&A, 96, 164
- de Carvalho, R. R., & da Costa, L. N. 1987, A&A, 171, 66
- de Jong, R. S. 1996, A&AS, 118, 557
- de Souza, R. E., & dos Anjos, S. 1987, A&AS, 70, 465
- de Zeeuw, P. T., et al. 2002, MNRAS, 329, 513
- Dettmar, R.-J., & Barteldrees, A. 1988, BAAS, 20, 1085
- D'Onofrio, M., Zaggia, S. R., Longo, G., Caon, N., & Capaccioli, M. 1995, A&A, 296, 319
- Dressler, A., & Sandage, A. 1983, ApJ, 265, 664
- Emsellem, E., & Arsenault, R. 1997, A&A, 318, L39
- Emsellem, E., Bacon, R., Monnet, G., & Poulain, P. 1996, A&A, 312, 777
- Emsellem, E., Greusard, D., Combes, F., Friedli, D., Leon, S., Pécontal, E., & Wozniak, H. 2001, A&A, 368, 52

- Emsellem, E., et al. 2004, MNRAS, in press.
- Englmaier, P., & Shlosman, I. 2000, ApJ, 528, 677
- Erwin, P., Beltrán, J. C. V., Graham, A. W., & Beckman, J. E. 2003, ApJ, 597, 929
- Erwin, P., & Sparke, L. S. 2002, AJ, 124, 65
- Erwin, P., & Sparke, L. S. 2003, ApJS, 146, 299
- Eskridge, P. B., et al. 2000, AJ, 119, 536
- Falcón-Barroso, J., et al. 2004, MNRAS, in press.
- Fisher, D. 1997, AJ, 113, 950
- Fisher, D., Franx, M., & Illingworth, G. 1996, ApJ, 459, 110
- Friedli, D., & Benz, W. 1993, A&A, 268, 65
- Friedli, D., & Benz, W. 1995, A&A, 301, 649
- Friedli, D., Benz, W., & Kennicutt, R. 1994, ApJ, 430, 105
- Gerhard, O. E. 1993, MNRAS, 265, 213
- Gerin, M., Combes, F., & Athanassoula, E. 1990, A&A, 230, 37
- Heller, C. H., & Shlosman, I. 1994, ApJ, 424, 84
- Heller, C. H., & Shlosman, I. 1996, ApJ, 471, 143
- Jarvis, B. J. 1986, AJ, 91, 65
- Jarvis, B. 1987, AJ, 94, 30
- Karachentsev, I. D., Karachentseva, V. E., & Parnovsky, S. L. 1993, Astron. Narchr., 314, 97
- Kormendy, J. 1982, ApJ, 257, 75
- Kormendy, J. 1993, in Galactic Bulges, eds. H. Dejonghe, & H. J. Habing (Dordrecht: Kluwer), 209
- Kormendy, J. 2001, Rev. Mex. A&A, Serie de Conferencias, 10, 69
- Kormendy, J., & Illingworth, G. 1982, ApJ, 256, 460

- Kuijken, K., & Merrifield, M. R. 1995, ApJ, 443, L13
- Larson, R. B. 1976, MNRAS, 176, 31
- Longo, G., Zaggia, S. R., Busarello, G., & Richter, G. 1994, ApJS, 105, 433
- Lütticke, R., Dettmar, R.-J., & Pohlen, M. 2000a, A&AS, 145, 405
- Lütticke, R., Dettmar, R.-J., & Pohlen, M. 2000b, A&A, 362, 435
- van der Marel, R. P., & Franx, M. 1993, ApJ, 407, 525
- MacArthur, L. A., Courteau, S., & Holtzman, J. A. 2003, ApJ, 582, 689
- Martin, P., & Roy, J.-R. 1994, ApJ, 424, 599
- Martinet, L., & Friedli, D. 1997, A&A, 323, 363
- Massey, P., & Foltz, C. B. 2000, PASP, 112, 566
- Mathewson, D. S., Ford, V. L., & Buchhorn, M. 1992, ApJS, 81, 413
- May, A., van Albada, T. S., & Norman, C. A. 1985, MNRAS, 214, 131
- Merrifield, M. R., & Kuijken, K. 1999, A&A, 443, L47
- Mihos, J. C., Walker, I. R., Hernquist, L., de Oliveira, M. C., & Bolte, M. 1995, ApJ, 447, L87
- Nishiura, S., Shimada, M., Ohyama, Y., Murayama, T., & Taniguchi, Y. 2000, AJ, 120, 1691
- Noguchi, M. 1987, MNRAS, 228, 635
- Norman, C. A., Sellwood, J. A., & Hasan, H. 1996, ApJ, 462, 114
- Patsis, P. A., Skokos, Ch., & Athanassoula, E. 2002, MNRAS, 337, 578
- Patsis, P. A., Skokos, Ch., & Athanassoula, E. 2003, MNRAS, 342, 69
- Pfenniger, D. 1984, A&A, 134, 373
- Pfenniger, D., & Friedli, D. 1991, A&A, 252, 75
- Pfenniger, D., & Norman, C. 1990, ApJ, 363, 391
- Raha, N., Sellwood, J. A., James, R. A., & Kahn, F. D. 1991, Nature, 352

- Rowley, G. 1986, Ph.D. Thesis, Australian National University
- Rowley, G. 1988, ApJ, 331, 124
- Rubin, V. C., Whitmore, B. C., & Ford, W. K. 1988, ApJ, 333, 522
- Rubin, V. C., Waterman, A. H., & Kenney, J. D. P. 1999, AJ, 118, 236
- Seifert, W., & Scorza, C. 1996, A&A, 310, 75
- Seigar, M. S., & James, P. A. 1998, MNRAS, 299, 672
- Sellwood, J. A., & Wilkinson, A. 1993, Rep. Prog. Phys., 56, 173
- Shaw, M. A. 1987, MNRAS, 229, 691
- Shaw, M. 1993a, A&A, 280, 33
- Shaw, M. 1993b, MNRAS, 261, 718
- Shaw, M. A., Dettmar, R. J., & Barteldrees, A. 1990, A&A, 240, 36
- Shaw, M., Wilkinson, A., & Carter, D. 1993, A&A, 268, 511
- Shen, J., & Sellwood, J. A. 2003, ApJ, in press.
- Shlosman, I., & Heller, C. H. 2002, ApJ, 565, 921
- Skokos, Ch., Patsis, P. A., & Athanassoula, E. 2002a, MNRAS, 333, 847
- Skokos, Ch., Patsis, P. A., & Athanassoula, E. 2002b, MNRAS, 333, 861
- Sparke, L. S., & Sellwood, J. A. 1987, MNRAS, 225, 653
- Tonry, J., & Davis, M. 1979, AJ, 84, 1511
- Wakamatsu, K.-I., & Hamabe, M. 1984, ApJS, 56, 283
- Wozniak, H. 1994, A&A, 286, L5
- Wozniak, H., Friedli, D., Martinet, L., Martin, P., & Bratschi, P. 1995, A&AS, 111, 115

Zaritsky, D., Kennicutt, R. C., Jr., Huchra, J. P. 1994, ApJ, 420, 87

This preprint was prepared with the AAS IATEX macros v5.2.

Fig. 1.— Stellar kinematics of galaxies with a B/PS bulge and no or confined emission. From top to bottom, the panels show an optical image of the galaxy from the Digitized Sky Surveys (with isophotal contours), and the registered V, σ , h_3 , and h_4 profiles along the major-axis. The spatial scale varies from galaxy to galaxy but the kinematic limits are fixed. The measurements were folded about the center and the errors represent half the difference between the approaching and receding sides. Measurements are mirrored and denoted by a cross without an error bar when available from one side only. The data were binned to $S/N \geq 5$ per spatial and spectral element for V and σ and $S/N \geq 10$ for h_3 and h_4 . The final S/N are thus at least 7 and 14, respectively.

Fig. 2.— Same as Figure 1 but for the galaxies with a B/PS bulge and extended emission (main sample of Bureau & Freeman 1999).

Fig. 3.— Same as Figure 1 but for the galaxies of the control sample (control sample of Bureau & Freeman 1999).

Fig. 4.— Velocity dispersion of all sample galaxies derived using the entire spectral range (solid circles) and the Mg b region only (crosses). Errors bars are not plotted for clarity.

Fig. 5.— Comparison of our stellar measurements with published stellar kinematics. Data from this paper are shown as filled circles and literature data as asterisks and boxes. Error bars are drawn when available and references are available in the text.

Fig. 6.— Same as Figure 5 but for the published gas kinematics.

Fig. 7.— Rotational and pressure support for all sample galaxies. The dimensionless parameter V/σ is shown as a function of projected radius. Crosses without an error bar denote data available from one side only.

Fig. 8.— Velocity profile asymmetries for all sample galaxies. The LOSVD asymmetry (skewness) h_3 is shown as a function of V/σ . Data with $S/N \ge 10$ were used here for both V, σ , and h_3 . Crosses without an error bar denote data available from one side only. The points are connected as a function of projected radius.

Fig. 9.— A schematic view of the kinematic profiles for V, σ , and h_3 derived for most sample galaxies.

Table 1.	General properties of sample galax	ies.

Galaxy	R.A.(2000)	Dec.(2000)	Type	B_{T}	D_{25}	$V_{\rm hel}$	$M_B^{\rm c}$	Environment	Note
	h m s	0		mag	arcmin	$\rm km~s^{-1}$	mag		
(1)	$(2)^{a}$	$(3)^{\mathbf{a}}$	$(4)^{b}$	$(5)^{\mathbf{a}}$	$(6)^{a}$	$(7)^{\mathrm{a}}$	$(8)^{\mathrm{a}}$	$(9)^{c}$	$(10)^{\circ}$
Galaxies with	no or confine	d emission							
NGC 1381	03 36 31.7	-35 17 43	SA0	12.7	2.63	1776	-19.2	Cluster	
NGC 1596	$04 \ 27 \ 37.8$	-55 01 37	SA0	12.0	3.89	1509	-19.3	Group	
NGC 2310	06 53 53.8	-40 51 46	SO	12.6	4.16	1187	-18.6	Isolated	
ESO 311-G012	$07 \ 47 \ 34.0$	-41 27 07	S0/a?	12.4	3.71	1130	-20.0	Isolated	
NGC 3203	$10 \ 19 \ 34.4$	-26 41 53	$SA(r)0^{+}?$	13.0	2.81	2410	-19.9	Group	
IC 4767	18 47 41.6	-63 24 20	S pec	14.3	1.51	3544	-19.5	Cluster	
ESO 185-G053	$20 \ 03 \ 00.4$	-55 56 53	SB pec	14.3	1.23	4475	-20.0	Cluster	
Galaxies with	extended em	ission							
NGC 128	$00 \ 29 \ 15.1$	+02 51 50	S0 pec	12.7	2.81	4228	-21.4	Group	
ESO 151-G004	00 56 07.3	-53 11 28	$S0^{0}$	14.7	1.31	7456^{d}	-20.4 ^d	Group	
NGC 1886	$05 \ 21 \ 48.2$	-23 48 36	Sab	13.8	3.23	1737	-19.2	Isolated	
NGC 2788A	$09 \ 02 \ 40.2$	-68 13 38	$^{\rm Sb}$	13.6	2.88	4056	-21.5	Cluster	Dust
IC 2531	09 59 55.4	-29 37 02	Sb	12.9	6.76	2474	-21.6	Cluster	Dust
NGC 3390	$10 \ 48 \ 04.4$	-31 32 02	$^{\rm Sb}$	12.8	3.46	3039	-21.5	Companions?	
NGC 4469	12 29 28.0	+08 44 59	SB(s)0/a?	12.4	3.46	576	-17.8	Cluster	
NGC 4710	12 49 38.9	+15 09 57	$SA(r)0^+$	11.9	4.89	1324	-19.8	Cluster	
PGC 44931	$13 \ 01 \ 49.5$	-08 20 10	Sbc	14.2	2.81	3804	-21.1	Isolated	
ESO 443-G042	$13 \ 03 \ 29.9$	-29 49 36	$^{\rm Sb}$	13.9	2.88	2912	-20.6	Companions?	Dust
NGC 5746	$14 \ 44 \ 55.9$	+01 57 17	SAB(rs)b?	11.4	6.91	1720	-21.8	Group	
NGC 6722	19 03 39.6	-64 53 41	Sb	13.5	2.88	5749	-22.2	Isolated	
NGC 6771	19 18 39.6	-60 32 46	$SA(r)0^+$?	13.6	2.34	4221	-20.5	Group	
IC 4937	$20 \ 05 \ 17.9$	-56 15 20	Sb	14.8	1.86	2337	-18.6	Cluster	Dust
ESO 597-G036	20 48 15.0	-19 50 58	$S0^0$ pec	15.2	0.87	8694	-20.7	Group	Dust
IC 5096	21 18 21.8	-63 45 42	Sb	13.6	3.16	3142	-20.7	Companions?	
ESO 240-G011	23 37 50.5	-47 43 37	Sb	13.4	4.89	2842	-21.0	Group	
Control sampl	e								
NGC 1032	02 39 23.6	$+01 \ 05 \ 38$	S0/a	12.7	3.46	2722	-20.7	Companions?	Dust
NGC 3957	11 54 01.5	-19 34 09	SA0 ⁺	13.0	3.09	1686	-19.0	Cluster	
NGC 4703	12 49 18.9	-09 06 30	$^{\rm Sb}$	14.0	2.45	4458	-21.1	Isolated	Dust
NGC 5084	13 20 16.8	-21 49 38	SO	11.5	10.71	1725	-20.9	Cluster	
NGC 7123	21 50 46.4	-70 19 59	Sa	13.6	2.51	3737	-20.3	Isolated	Dust
IC 5176	$22 \ 14 \ 55.3$	-66 50 56	SAB(s)bc?	13.4	4.36	1746	-19.6	Companions?	

^aParameters from LEDA (Lyon-Meudon Extragalactic Database).

^bMorphological classifications from Jarvis (1986), de Souza & dos Anjos (1987), Shaw (1987), and Karachentsev et al. (1993).

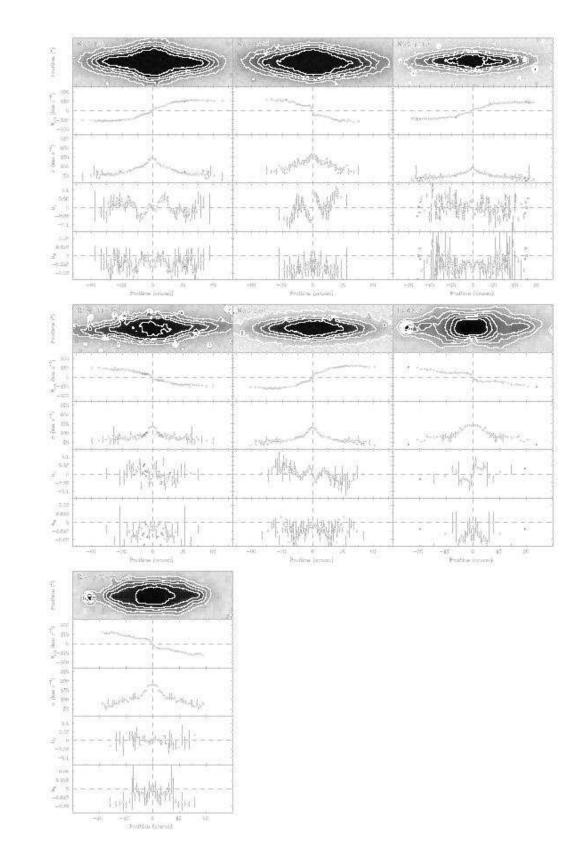
^cNotes by Bureau (1998) and Bureau & Freeman (1999).

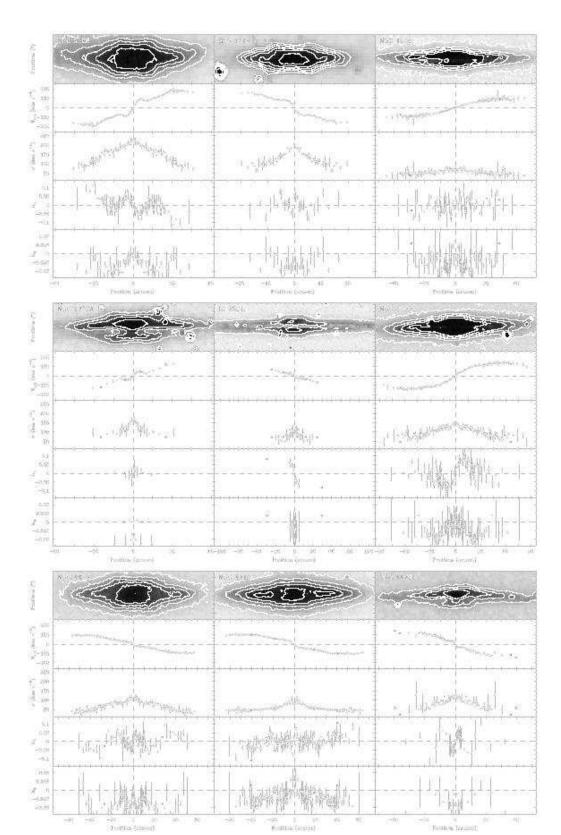
 $^{\rm d}{\rm Redshift}$ and corrected absolute B magnitude from this study.

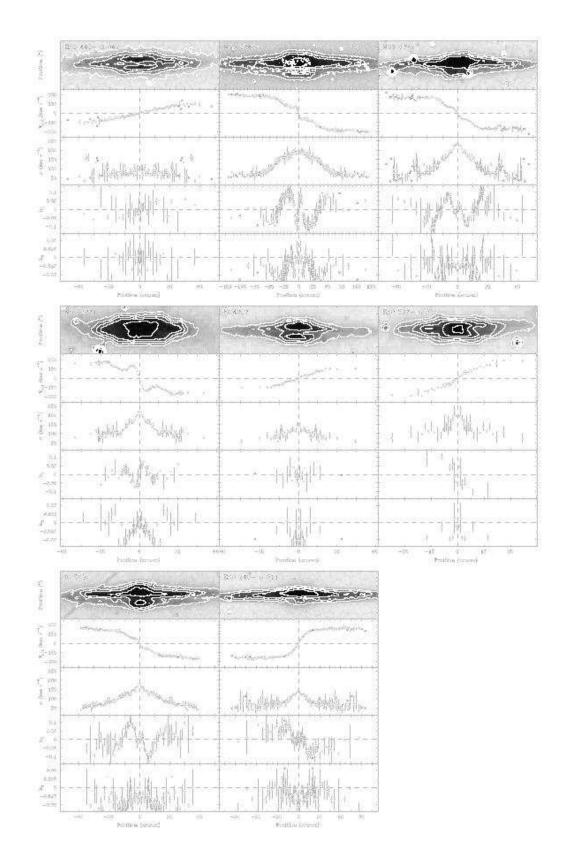
	Lütticke et al. (2000a)	Bureau & I	Freeman (1999)	This work
Galaxy	Classification code ^a	(DSS)	Gas PVD	Stellar Kinematic
Galaxies with	no or confined emission			
NGC 1381	2.0	Boxy		Bar
NGC 1596	4.0	Boxy		Bar
NGC 2310	2.0	Boxy		Bar
ESO 311-G012	2.0	Boxy		Bar
NGC 3203	3.0	Boxy		Bar
IC 4767	1.0	Peanut		Bar
ESO 185-G053	2.0	Peanut		Bar
Galaxies with	extended emission			
NGC 128	1.0	Peanut	Bar	Bar
ESO 151-G004	1.0	Peanut	Bar	Bar
NGC 1886	1.0	Peanut	Bar	Bar
NGC 2788A	1.0	Peanut	Bar	Bar
IC 2531	1.0	Peanut	Bar	Bar
NGC 3390	2.0	Boxy	Accretion	Bar?
NGC 4469	1.0	Peanut	Axisymmetric	Bar
NGC 4710	1.5	Boxy	Bar	Bar
PGC 44931	1.0	Peanut	Bar	Bar
ESO 443-G042	1.0	Peanut	Bar	Bar?
NGC 5746	1.0	Peanut	Bar	Bar
NGC 6722	1.0	Peanut	Bar	Bar
NGC 6771	1.0	Peanut	Bar	Bar
IC 4937	1.0	Peanut	Bar	Bar
ESO 597-G036	1.0	Peanut	Accretion	Bar
IC 5096	4.0	Boxy	Bar	Bar
ESO 240-G011	4.0	Boxy	Bar	Bar
Control sample	e			
NGC 1032	4.0	Spheroidal	Axisymmetric	No bar
NGC 3957	3.0	Spheroidal	Axisymmetric	Bar
NGC 4703	4.0	Spheroidal	Axisymmetric	Bar
NGC 5084	4.0	Spheroidal	Accretion	No bar
NGC 7123	4.0	Spheroidal	Accretion	Bar?
IC 5176	4.0	Spheroidal	Axisymmetric	No bar

Table 2. Bulge classifications and bar signatures.

^a1: peanut-shaped bulge; 1.5: bulge boxy-shaped on one side and peanut-shaped on the other; 2: box-shaped bulge; 3: bulge is close to box-shaped, not elliptical; 4: elliptical bulge.







· · · · · · · · · · · · · · · · · · ·		
1. The first the plant	appendit and a second	1. 1 in March and Mary 1.
	-19 -3 L A 19 Realize prices	-40 -52 a pa 40 Pointe Istual
	-	Sector Sector
·		
·		

